Available online at www.sciencedirect.com
ScienceDirect
Catalysis Today 118 (2006) 315–322
CATALYSIS TODAY
www.elsevier.com/locate/cattod

The structures of VO_x/MO_x and alkali-VO_x/MO_x catalysts and their catalytic performances for soot combustion

Jian Liu [a], Zhen Zhao [a,*], Chunming Xu [a], Aijun Duan [a], Ling Zhu [b], Xuezhong Wang [b]

[a] State Key Laboratory of Heavy Oil Processing, Faculty of Chemical Science and Engineering, China University of Petroleum, 18# Fuxue Road, Chang Ping, Beijing 102249, China
[b] The Chinese Research Academy of Environmental Sciences, Beijing 101200, China

Available online 22 August 2006

Abstract

Vanadium oxides supported on γ-Al_2O_3, SiO_2, TiO_2, and ZrO_2 were studied on their molecular structures and reactive performances for soot combustion. To investigate the effect of different alkali metals on the structures and reactivities of supported-vanadium oxide catalysts, they were doped into the V_4/TiO_2 catalyst which had the best intrinsic activity for soot combustion in the selected supported vanadium oxide catalysts. The experimental results demonstrated that the catalytic properties of these catalysts depended on the vanadium loading amount, support nature, and the presence or the absence of alkali metals. The spectroscopic analysis (FT-IR and UV–vis) and H_2-TPR results revealed that the higher activity of alkali-promoted vanadium oxide catalysts could be related to the ability of alkali metal promoting the redox cycle of the active vanadyl species. TG results showed that adding alkali to V_m/TiO_2 catalyst was beneficial to lowering their melting points. Low melting points could ensure the good surface atom migration ability, which would improve the contact between the catalyst and soot. Due to the alkali metal components promoting the redox ability and the mobility of the catalysts, alkali-modified vanadium oxide catalysts could remarkably improve their catalytic activities for soot combustion. The catalytic activity order for soot combustion followed Li > Na > K > Rb > Cs in the catalyst system of alkali-V_4/TiO_2, and the reason why it followed this sequence was discussed.

Keywords: Supported vanadium oxide; Soot; Combustion; Alkali metal; Catalyst

1. Introduction

Soot emitted from diesel engines is a serious contamination in urban areas. Its emission can be reduced in various ways. Collection of soot in a monolithic filter and simultaneous combustion is considered to be a good option to minimize the environmental contamination. However, soot combustion takes place at temperatures of 550–600 °C, while the temperature of diesel exhaust is typically 200–400 °C. Hence, an active oxidation catalyst is needed to prevent accumulation of soot in the monolithic filter [1,2]. Supported vanadium oxide catalysts are widely used as catalysts in oxidation reactions, e.g., the oxidation of sulfur dioxide, carbon monoxide, and hydrocarbons [3–7]. In our previous work, we have reported that supported vanadium oxides and K-promoted vanadium oxides were the good candidate catalysts for diesel soot oxidation [8]. Their high activity in the oxidation of soot has been related to its low melting point, which ensured a good contact between the soot and catalyst [9–11]. However, there are still some unknown points. For example, what are the relations among the catalytic performances of supported alkali-modified vanadia catalysts for diesel soot combustion reaction and their compositions, structure, and support nature?

Potassium has been utilized as promoted catalysts for both coal gasification and combustion, and these reactions are expected to take place with a mechanism that is analogous to soot combustion [12]. Some authors agree that potassium exhibits the following positive effects on the soot combustion: firstly, potassium increases the oxygen reactivity of M=O bond as an electron donor. Secondly, potassium enhances the reaction by forming low melting compounds (KOH, KNO_3) or eutectics with other components of the catalyst that increase the catalyst–soot contact. Thirdly, potassium promotes the formation of a superficial carbonate intermediate by reaction with the CO_2

* Corresponding author. Tel.: +86 10 89731586 (O).
E-mail address: zhenzhao@cup.edu.cn (Z. Zhao).

0920-5861/$ – see front matter © 2006 Elsevier B.V. All rights reserved.
doi:10.1016/j.cattod.2006.07.015

produced during combustion [13–15]. However, as far as we know, few papers in open literature studied on different alkali metal modified vanadium oxide catalysts, and there is also few reports on the correlating the molecular structure of supported alkali-promoted vanadium oxide catalysts and their catalytic performances for soot combustion.

Based on our previous work [8], three issues concerning the structure of the supported vanadium oxide or alkali-modified vanadium oxide catalysts were further investigated by means of thermal analysis technique and spectroscopic characterization. The first one is the effect of the concentration of active component. The second one is the effect of support nature, and the third one is the effect of reducibility. This study especially addresses the different catalytic activities of different alkali-modified vanadate catalysts for soot combustion and the reason for the difference. The aim is to establish the relationship between the structures and catalytic reactivity of the studied catalysts in molecular level.

2. Experimental

2.1. Catalyst preparation

NH_4VO_3 was used as starting material containing V and alkali metals were introduced using their corresponding nitrates. The support metal oxides were γ-Al_2O_3 (40–60 mesh, 179 m^2/g), SiO_2 (60–80 mesh, 342 m^2/g), TiO_2 (rutile, 9 m^2/g), and ZrO_2 (60–100 mesh, 2 m^2/g). All of the chemicals used for catalyst preparation were of analytical grade. The samples were prepared by an incipient-wetness impregnation method with a variable NH_4VO_3 contents between 0 and 20%, which were generically named as V_m/MO_x, where MO_x stands for support, and m is the molar ratio of 100V to support MO_x (m = 0, 0.1, 1, 4, 10, and 20). Similarly, the binary catalysts were prepared by simultaneous impregnation of V and alkali metal as the molar ratio V:A:M = 4:4:100, which were generically named as A_4V_4/MO_x, where A stands for alkali metal (Li, Na, K, Rb, and Cs). During the impregnation, the citric acid (equi-molar to metal vanadium) was added to the solution for promoting the dissolution of NH_4VO_3. After the impregnation step, the samples were dried at 120 °C for 12 h. Finally, the samples were calcined at 700 °C for 4 h in static air.

2.2. Catalyst characterization

TG-DTA analyses were performed by a Rigaku TAS-300 thermobalance. Typically, 10 mg catalyst was put in the sample holder inside an aluminium crucible, using an empty crucible in the reference holder. The sample was submitted to a linear rise of temperature from 100 to 800 °C with a heating rate of 10 °C/min under an air flow. H_2-TPR measurements were performed in a conventional flow apparatus. The catalyst sample was loaded in a Quartz tube (d_i = 6 mm) and pretreated at 600 °C in flowing air for 30 min. After cooling in a helium flow down to 100 °C, the helium gas was switched to a 10% H_2/He gas mixture. The temperature was then ramped from 100 to 900 °C at a heating rate of 10 °C/min in 10% H_2/He with a constant flow rate of 40 cm^3/min. An on-line thermal conductivity detector (TCD) was used to record H_2 consumption.

The FT-IR absorbance spectra were recorded on a FTS-3000 spectrophotometer manufactured by American Digilab company. Two hundred milligrams pellet was produced by pressing a mixture of each treated catalyst and KBr (1:100 weight ratio). A resolution of 2 cm^{-1} and 64 scans were applied to obtain the spectra. The spectra are displayed without any further data processing. UV–vis absorption spectra of the samples after H_2-TPR were performed on a spectrophotometer (Hitachi U-4100) equipped with the integration sphere diffuse reflectance attachment. The standard support reflectance was used as the baseline for the corresponding catalyst measurement.

2.3. Catalytic activity measurement

To evaluate the catalytic performance for diesel soot combustion under simulated diesel gas conditions, a series of TPO reactions were carried out on a fixed-bed tubular quartz system. The reaction temperature was controlled through a PID-regulation system based on the measurements of a K-type thermocouple and varied during each TPO run from 200 to 700 °C at a 2 °C/min increasing rate. Printex-U supplied by Degussa was used as a model soot (primary particle size = 25 nm, specific surface = 100 m^2/g). The mixture of catalyst and soot in a mass ratio 10:1 was carried out during 10 min in an agata mortar, and 100 mg of the mixture placed in the tubular quartz reactor (d_i = 6 mm) for each test. Reactant gases containing 5% O_2 and 2000 ppm NO balanced with He were passed through a mixture of the catalyst and soot at a flow rate of 200 ml/min (STP). The outlet gas composition coming from the reactor were analyzed by an on-line gas chromatograph (GC) used both TCD and FID detectors. The TCD was used to measure the concentration of O_2, N_2, CO, and NO after separating these gases through a molecular sieve 5A column. The FID was employed to determine CO and CO_2 concentrations after separating these gases over a Porapak N column and converting them to CH_4 over a nickel catalyst at 380 °C.

3. Results

3.1. Catalyst characterization

3.1.1. TG-DTA analyses

The TG-DTA profiles of V_4/MO_x and A_4V_4/TiO_2 catalysts are shown in Fig. 1(a and b), respectively. On the V_4/Al_2O_3 and V_4/SiO_2 catalysts, no any endothermic peak was observed. On the V_4/TiO_2 sample, an endothermic peak at approximately 670 °C was found, and on the V_4/ZrO_2 sample an endothermic peak at 755 °C was obtained. These results reveal that the melting point order follows $V_4/SiO_2 \sim V_4/Al_2O_3 > V_4/ZrO_2 > V_4/TiO_2$. In Fig. 1(b), the TG-DTA diagrams of A_4V_4/TiO_2 catalysts are plotted for comparison. Li_4V_4/TiO_2 shows three endothermic peaks at 370, 410, and 590 °C. K_4V_4/TiO_2 shows three endothermic peaks at 140, 405, and 510 °C. The endothermic peak at 140 °C is due to the evaporation of combined H_2O. Moreover, an endothermic peak at 600 °C was observed on the

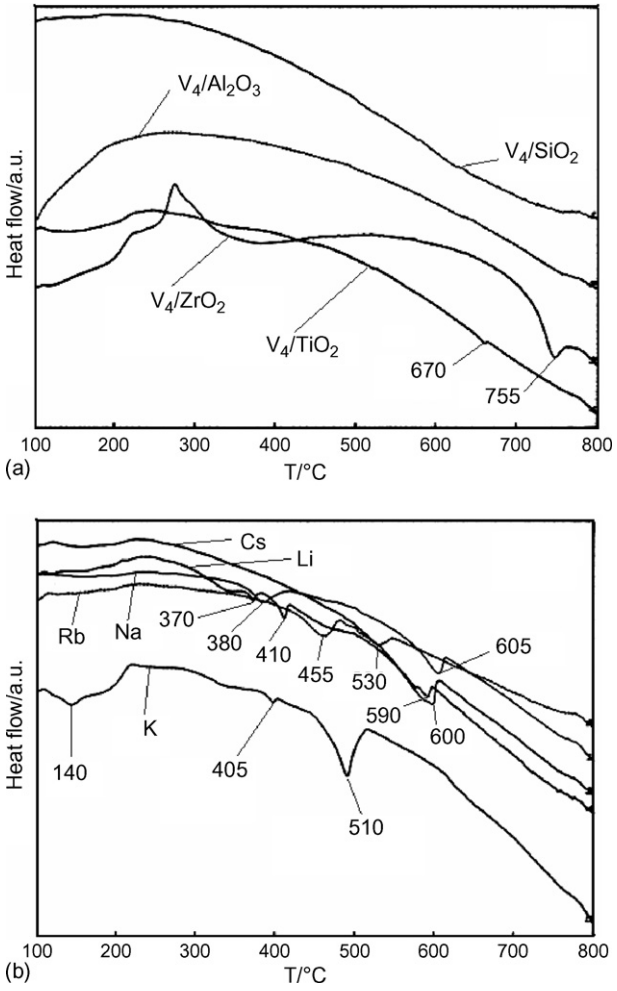

Fig. 1. The TG-DTA analyses of V_4/MO_x and A_4V_4/TiO_2 (A = Li, Na, K, Rb, Cs): (a) V_4/MO_x and (b) A_4V_4/TiO_2.

Cs_4V_4/TiO_2 sample. In addition, Na_4V_4/TiO_2 exhibits two endothermic peaks at 380 and 605 °C, and Rb_4V_4/TiO_2 exhibits two endothermic peaks at 455 and 530 °C, respectively. Compared with the result of V_4/TiO_2 TG-DTA, it can be concluded that adding alkali to V_m/TiO_2 catalyst is beneficial to lowering their melting points. Furthermore, considering the lowest endothermic temperature the sequence of the melting point for A_4V_4/TiO_2 catalyst follows Cs > Rb > K > Na > Li (600, 455, 405, 380, and 370 °C, respectively) if the endothermic peak at 140 °C was excluded which is due to the evaporation of combined H_2O. These results indicate that Li_4V_4/TiO_2 catalyst probably had the best atom migration ability in A_4V_4/TiO_2 system because it had the lowest melting point.

3.1.2. H_2-TPR measurements

H_2-TPR profiles of V_m/MO_x catalysts are showed in Fig. 2. The temperature at which the reduction starts (T_{red}) was taken as a measure of the reducibility of the catalytic system. The lower T_{red} is, the stronger is the oxidizing ability of the catalyst. Fig. 2 shows that all $V_{0.1}/MO_x$ samples were neither the reduction peak nor the hydrogen consumption with the changing of reduction temperature, indicating that the oxidizing ability of these catalysts was very weak at low V loading. For V_m/Al_2O_3 catalysts, only one reduction peak (T_{red} = 503 °C) was observed on V_1/Al_2O_3 catalyst. Instead, two reduction peaks were obtained for V_4/Al_2O_3, V_{10}/Al_2O_3, and V_{20}/Al_2O_3 (T_{red} = 394 and 603, 342 and 655, and 618 and 736 °C, respectively). The first reduction peak may be attributed to the reduction of polyvanadate species, and the second one may be related to the reduction of crystalline V_2O_5 [16]. These results reveal that V_{10}/Al_2O_3 had the best oxidibility among V_m/Al_2O_3 catalyst system. For V_m/SiO_2 samples, no reduction peak was observed on V_1/SiO_2 and only a reduction peak was obtained for V_4/SiO_2, V_{10}/SiO_2, and V_{20}/SiO_2 (T_{red} = 721, 704, and 731 °C, respectively). These results indicate that V_{10}/SiO_2 had the best oxidizing ability among V_m/SiO_2 catalyst systems. For V_m/TiO_2 samples, no reduction peak was observed on V_1/TiO_2 and only one reduction peak was obtained for V_4/TiO_2 (T_{red} = 765 °C). However, two reduction peaks were obtained for V_{10}/TiO_2 and V_{20}/TiO_2 (T_{red} = 744 and 816, and 555 and 767 °C, respectively). For V_m/ZrO_2 catalysts, only one reduction peak was observed on V_1/ZrO_2 and V_4/ZrO_2 (T_{red} = 731 and 686 °C, respectively). However, three reduction peaks were obtained for V_{10}/ZrO_2 (T_{red} = 579, 745, and 827 °C). Moreover, V_{20}/ZrO_2 exhibits two reduction peaks at 583 and 810 °C. These results reveal that V_4/TiO_2 and V_4/ZrO_2 had the best oxidizing ability among V_m/TiO_2 and V_m/ZrO_2 catalyst systems, respectively.

The H_2-TPR profiles of A_4V_4/TiO_2 system are shown in Fig. 3. Their TPR profiles exhibit a complex pattern due to the complicate alkali-vanadium oxide species, but the reduction temperatures were obviously shifted towards lower values as alkali metals were added into V_4/TiO_2 catalyst. Therefore, doping vanadium oxide catalysts with alkali metals increased the reducibility of the V_4/TiO_2 catalyst.

3.1.3. FT-IR characterization

Some useful information has been given in our previous studies about FT-IR spectroscopy of V_m/MO_x catalysts [8]. Although support materials showed strong absorption bands below 1200 cm^{-1}, some interesting vibration bands originated from the catalytic surface material were still observed. The structure of supported vanadia exposed to ambient air depended on the support material and on the V loading [17–20]. For the V_m/Al_2O_3 and V_m/TiO_2 samples, V_{10}/Al_2O_3 and V_{10}/TiO_2 existed a small vibration band at around 1020 cm^{-1} originated from the V=O stretch vibration of V_2O_5, but V=O stretching vibration bands in the lower frequency range (1000–900 cm^{-1}) which were assigned to the V=O stretch vibration of polymeric vanadyl species or V_xO_y "clusters" formed on the surface and V–O–V stretching vibration bands below 900 cm^{-1} bands were not detected in all V_m/Al_2O_3 and V_m/TiO_2 catalysts. For the V_m/SiO_2 sample, it is noted that a new broad band at around 929 cm^{-1} originated from V=O stretch vibration in VO_x "cluster" appeared on V_{10}/SiO_2 and V_{20}/SiO_2 catalysts. The differences between the results obtained in this work and those of described in the other cited literature [18–19] in relation to the FT-IR spectra of V_m/SiO_2 samples may be due to the different preparation details that we used the citric acid to promote the solubility of NH_4VO_3. In an acid solution

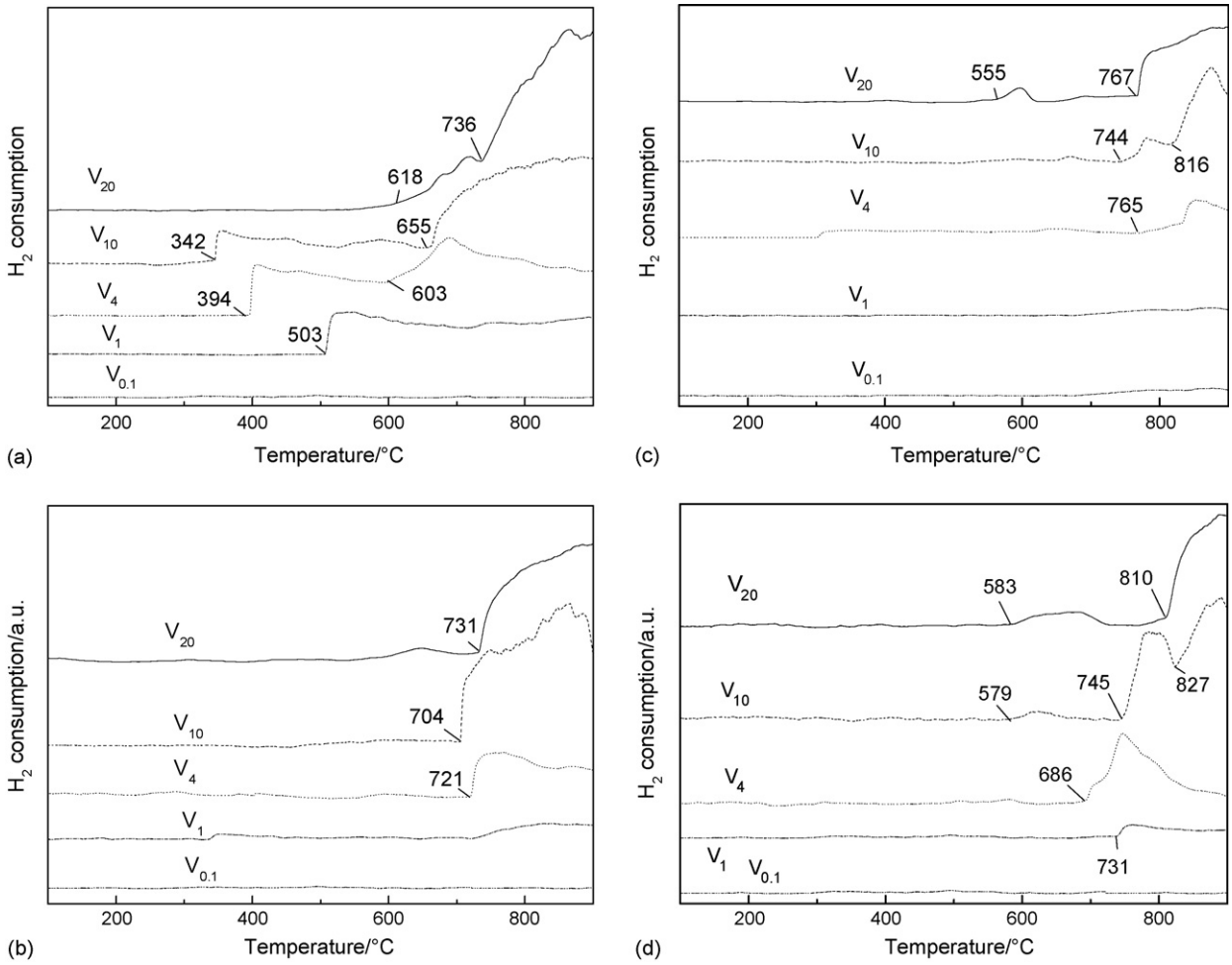

Fig. 2. The H_2-TPR profiles of V_m/MO_x ($m = 0.1$, 1, 4, 10, 20): (a) V_m/Al_2O_3; (b) V_m/SiO_2; (c) V_m/TiO_2; (d) V_m/ZrO_2.

attributing to the effect of complex agent, citric acid, some amounts of VO_x "cluster" formed in the V_{10}/SiO_2 and V_{20}/SiO_2 catalysts. Some groups have also detected the V=O stretch vibration at 940 cm^{-1} in the high loading of V_m/SiO_2 samples [20–22]. But no absorption band was observed below 900 cm^{-1} originated from V–O–V stretching vibration in all V_m/SiO_2 catalysts. For the V_m/ZrO_2 samples, V_4/ZrO_2, V_{10}/ZrO_2, and V_{20}/ZrO_2 show several peaks at 989, 946, 792, and 697 cm^{-1}. These results indicate that polyvanadate species had formed on the surface of V_m/ZrO_2 catalysts. But no V=O stretching vibration band at 1020 cm^{-1} was observed for V_m/ZrO_2 samples.

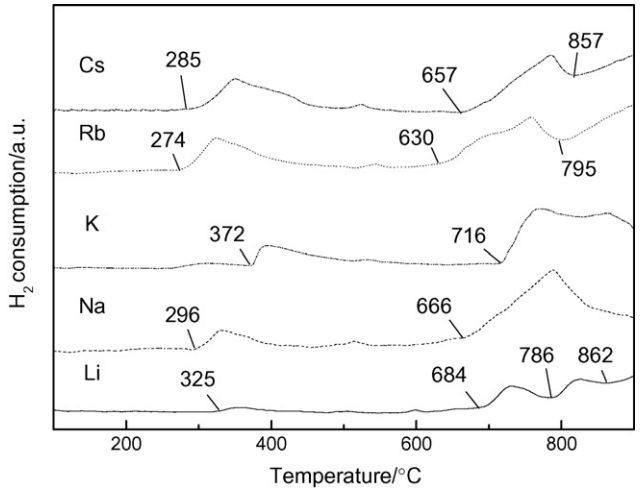

Fig. 3. The H_2-TPR profiles of A_4V_4/TiO_2 (A = Li, Na, K, Rb, Cs).

Fig. 4 shows that the FT-IR spectra of A_4V_4/TiO_2 catalysts. The IR spectra of all samples became flatter above 1000 cm^{-1} after doping alkali metals into V_4/TiO_2 catalyst. For comparison, the IR spectra of KVO_3 and KNO_3 are also shown in Fig. 4. Two absorption peaks at 968 and 917 cm^{-1} appeared in the spectra which were due to the V=O stretching vibration of AVO_3 produced in the A_4V_4/TiO_2 catalysts, whereas the very tiny absorption peak at 1386 cm^{-1} may be ascribed to the trace amount of nitrates existing on the surface of support [23,24]. A small amount of high disperse nitrates can be existed on the surface of oxide support but not decomposed even at high temperature. This interesting phenomenon has also been reported in the recent literature for $KNO_3/Ce_{0.5}Zr_{0.5}O_2$ catalysts [25]. For Li_4V_4/TiO_2 sample, a new absorption peak at 420 cm^{-1} cannot be assigned from the literatures that we have known. It is noted that the addition of the alkali metal to V_4/TiO_2 sample made the V=O stretching vibration shift to lower wave number.

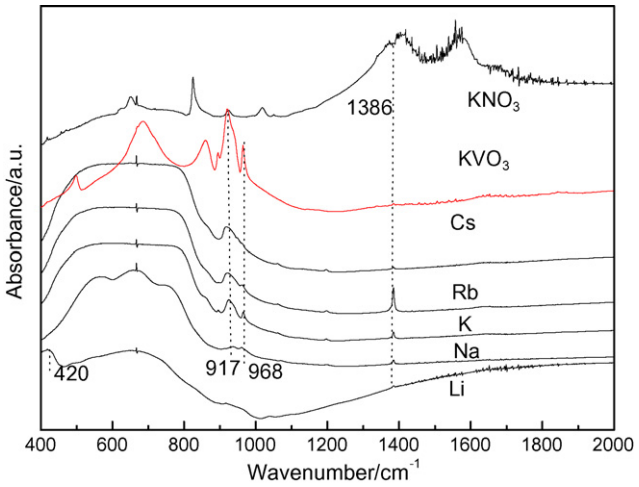

Fig. 4. The FT-IR spectra of A_4V_4/TiO_2 (A = Li, Na, K, Rb, Cs), KVO_3, and KNO_3.

3.1.4. UV–vis characterization

In order to further compare the reduction extent of the measured samples, the UV–vis spectra of the V_m/Al_2O_3 and V_m/SiO_2 samples after H_2-TPR were recorded. The spectra of V_m/TiO_2 and V_m/ZrO_2 samples after H_2-TPR were not recorded because the strong absorptions of TiO_2 and ZrO_2 supports cause their UV–vis signals very weak when the standard support reflectance was used as the baseline for the corresponding catalysts.

UV–vis diffuse reflectance spectroscopy has been widely used to investigate the structures and oxidation states of vanadium-containing solid oxides that possess the ligand-to-metal charge transfer (LMCT) transition of V^{5+} in the region of 550–200 nm and d-d transition of V^{4+} and V^{3+} in the range of 400–1000 nm [26]. In the region of 400–600 nm, the V ions with different valences (3^+, 4^+, and 5^+) can exist. And it is also difficult to distinguish the V^{4+} and V^{3+} d–d electron transition bands since these bands are located in the same range and tend to be broad and weak. However, V^{5+} can be distinguished from V^{4+} and V^{3+}. The bands 200–400 and 600–800 nm are the characteristic absorption bands for V^{5+} and V^{4+}/V^{3+}, respectively. Therefore, the ratio of the d–d electron transition band area of V^{4+}/V^{3+} (600–800 nm) to the area of LMCT band of V^{5+} (200–400 nm) was chosen as a parameter to relatively quantify the extent of reduction of V^{5+} cations in this study [26–28].

Fig. 5(a and b) shows the UV–vis spectra of V_m/Al_2O_3 and V_m/SiO_2 samples after H_2-TPR, respectively. The ratio of absorption band area (600–800 nm) to the band area (200–400 nm) was calculated and listed in Table 1. For comparison, the ratios of the corresponding absorption band areas of those samples before TPR are also listed in Table 1. It can be seen, from Fig. 5 and Table 1, that a very small amount of V^{4+}/V^{3+} was present on the samples with medium or high vanadium loading before TPR. The ratio of the absorption band area (600–800 nm) to the band area (200–400 nm) was very small at low vanadium loading indicating that a small fraction of V^{5+} was reduced to V^{4+}/V^{3+} during reduction. It increased with the increasing of vanadium loading suggesting that the extent of reduction increased with the increasing of vanadium loading.

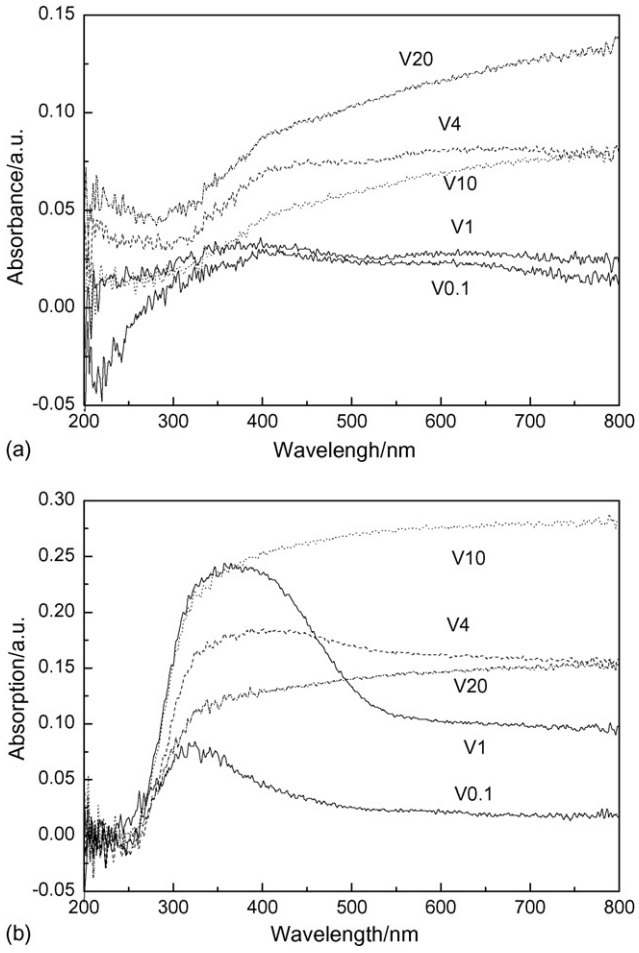

Fig. 5. The UV–vis spectra of V_m/MO_x after H_2-TPR (m = 0.1, 1, 4, 10, 20): (a) V_m/Al_2O_3 and (b) V_m/SiO_2.

3.2. Catalytic activity results

The soot conversion was calculated by integration of CO and CO_2 concentrations during the recorded time period. The amounts of CO and CO_2 were added and then the sum was multiplied by the gas flow rate (200 ml/min), converted from ml to mg "carbon", and divided by the amount of soot initially added. The carbon balance was always close to 95%, i.e., not

Table 1
The ratio of d–d electron transition band area of V^{4+}/V^{3+} (600–800 nm) to the area of LMCT band of V^{5+} (200–400 nm) of V_m/Al_2O_3 and V_m/SiO_2 before and after H_2-TPR (m = 0.1, 1, 4, 10, 20)

Catalyst	Ratio before TPR	Ratio after TPR
$V_{0.1}/Al_2O_3$	0.01	0.03
V_1/Al_2O_3	0.02	1.22
V_4/Al_2O_3	0.42	1.91
V_{10}/Al_2O_3	0.66	3.41
V_{20}/Al_2O_3	0.72	2.18
$V_{0.1}/SiO_2$	0.02	0.44
V_1/SiO_2	0.04	0.78
V_4/SiO_2	0.19	1.78
V_{10}/SiO_2	0.31	2.18
V_{20}/SiO_2	0.34	2.34

Table 2
The catalytic performances of V_m/MO_x for soot combustion (m = 0, 0.1, 1, 4, 10, 20)

	Catalyst					
	Al_2O_3	$V_{0.1}/Al_2O_3$	V_1/Al_2O_3	V_4/Al_2O_3	V_{10}/Al_2O_3	V_{20}/Al_2O_3
(a) V_m/Al_2O_3						
T_{10} (°C)	448	464	415	387	374	379
T_{50} (°C)	534	566	533	515	457	451
T_{90} (°C)	598	602	586	555	485	476
	Catalyst					
	SiO_2	$V_{0.1}/SiO_2$	V_1/SiO_2	V_4/SiO_2	V_{10}/SiO_2	V_{20}/SiO_2
(b) V_m/SiO_2						
T_{10} (°C)	435	456	413	392	369	376
T_{50} (°C)	548	563	529	511	471	464
T_{90} (°C)	600	592	567	556	524	521
	Catalyst					
	TiO_2	$V_{0.1}/TiO_2$	V_1/TiO$_2$	V_4/TiO_2	V_{10}/TiO_2	V_{20}/TiO_2
(c) V_m/TiO_2						
T_{10} (°C)	422	374	352	336	337	341
T_{50} (°C)	539	488	412	390	398	395
T_{90} (°C)	581	528	444	424	425	438
	Catalyst					
	ZrO_2	$V_{0.1}/ZrO_2$	V_1/ZrO_2	V_4/ZrO_2	V_{10}/ZrO_2	V_{20}/ZrO_2
(d) V_m/ZrO_2						
T_{10} (°C)	418	416	407	344	346	354
T_{50} (°C)	529	526	468	405	415	411
T_{90} (°C)	573	573	499	456	446	439

approaching complete conversion, which may ascribe to a little amount soot being oxidized at the low temperature (<200 °C). The catalytic activity was evaluated by the values of T_{10}, T_{50}, and T_{90}, which were defined as the temperatures at which 10, 50, and 90% of the soot were oxidized, respectively, during the TPO procedure. Since in practical applications the rate of carbon oxidation at lower temperatures is more important than the whole TPO profile, we especially focus on the results of T_{10}.

Tables 2 and 3 show the TPO results for the soot catalytic combustion. From these data, it is interesting to observe that the changes had same trends for T_{10}, T_{50}, and T_{90}. Furthermore, Table 2 shows that T_{10}, T_{50}, and T_{90} decreased as vanadium loading increasing at low V loading for the V_m/MO_x samples.

Table 3
The catalytic performances of A_4V_4/TiO_2 for soot combustion (A = Li, Na, K, Rb, Cs)

	Catalyst				
	Li_4V_4/TiO_2	Na_4V_4/TiO_2	K_4V_4/TiO_2	Rb_4V_4/TiO_2	Cs_4V_4/TiO_2
T_{10} (°C)	299	306	309	310	337
T_{50} (°C)	347	372	354	360	376
T_{90} (°C)	377	409	382	388	407

The catalytic activity order for soot combustion followed Ti > Zr > Al > Si comparing with these different support systems. For blank case (i.e., without catalyst) the soot combustion temperatures, T_{10}, T_{50}, and T_{90} were 482, 585, and 646 °C, respectively. Thus, the data in Table 2 reveal that V_m/MO_x catalysts could improve the activity of soot combustion, and V_4/TiO_2 was the most active catalyst for soot combustion among the all selected V_m/MO_x samples. It is noted that the catalytic activity order for soot combustion on different carrier-supported vanadia catalyst system was a little different from that in our previous report [8]. It is due to that the catalytic activity was evaluated by different methods. In the previous study T_{ig} and T_m were used to evaluate the catalytic performances of the catalysts for soot combustion, which was only considered the effect of the main product CO_2 in the soot combustion process. However, the amounts of byproduct CO produced in the soot combustion process have also been calculated into the reactive activity in the present studies. The selectivity of soot combustion was of difference for the various supported vanadium oxide catalysts. Thus, it caused a little change for the activity order. Moreover, the catalytic activity decreased a little for $V_{0.1}/Al_2O_3$ and $V_{0.1}/SiO_2$ in relation to the support materials. This phenomenon may be related to the low catalytic activity of isolated vanadia and the large internal porous specific surface areas of γ-Al_2O_3 and SiO_2. On the one hand, isolated vanadia are less active for many reactions [20]. On the other hand, the soot particulates with large sizes cannot enter the internal pore of the catalysts, which lead to soot combustion only carrying out on the outer surface of the catalysts. The greater are the internal porous specific surface areas of the catalysts, the less of the active site amounts on outer surface are and thus the catalytic activities are lower. These two factors caused the catalytic performances of $V_{0.1}/Al_2O_3$ and $V_{0.1}/SiO_2$ samples are even lower than those of corresponding pure supports.

The promoting effect of alkali metal has been reported in the soot combustion on other catalysts [12–14]. For a better comparison of V_m/MO_x and alkali-promoted vanadium oxide catalyst systems, we doped alkali metal into the V_4/TiO_2 catalyst, which had the best intrinsic activities for soot combustion in the selected V_m/MO_x catalyst systems. From Table 3, it can be seen that T_{10} remarkably decreased and the catalytic activity order for soot combustion followed Li > Na > K > Rb > Cs in the A_4V_4/TiO_2 catalyst system. Among them Li_4V_4/TiO_2 catalyst gave the best catalytic activity, i.e., the lowest soot combustion temperature.

4. Discussion

4.1. The effects of the concentration of vanadium oxides, nature of the support, and the reducibility on the structure and catalytic performances of V_m/MO_x and alkali-V_m/MO_x catalysts

The data reported here confirm that FT-IR, UV–vis, and TPR were useful methods for the characterization of the supported vanadium or alkali-promoted vanadium oxide catalysts. On

different oxide supports, three types of surface vanadium oxide species were generally identified: isolated, polymeric, and micro-crystalline vanadium oxide species. The ratio of polymerized to isolated surface vanadate species depended on the V loading, the support surface and the specific nature of the support [29–31]. The primary structures of hydrated V_m/Al_2O_3 and V_m/TiO_2 detected by IR spectroscopy are polymeric vanadyl species and very small amount of crystalline V_2O_5. The proportion of V_2O_5 grows with increasing vanadium loading. The structure of hydrated VO_x/SiO_2 also changes with V Loading. At low V loading, only isolated vanadate species were observed. As V loading increases, VO_x ''cluster'' of the dispersed vanadia appear on V_{10}/SiO_2 and V_{20}/SiO_2 catalysts. In contrast, V_m/ZrO_2 are present primarily as polyvanadate species. Small amounts of $Zr_2V_2O_7$ are also evident in the samples of high V loading when vanadia is supported on ZrO_2. After adding alkali metals into V_m/TiO_2 catalysts, some alkali metal vanadate compounds (AVO_3, nitrates) with low melting points formed on the samples. It will enhance the contact between soot and the catalysts. Moreover, as shown in Fig. 2, TPR results reveal that the reduction temperatures of medium V loading ($m = 10$ or 4) are lower than those of low ($m < 4$) or high V loading ($m = 20$). It indicates that V_m/MO_x with medium V loading have better reducibility than that with low or high V loading. After alkali metals dope into V_m/TiO_2 samples, the reduction transforms remarkably to lower temperatures, indicating that alkali metals increase the oxygen reactivity of V–O or V=O bond as an electron donor [12].

In consistence with previous characterization results, as V loading is low the catalytic activities of all of V_m/MO_x samples for soot combustion are very low. It is due to the low catalytic activities of isolated monovanadate species. The catalytic activities increase with V concentration increasing at low vanadium loadings, which is attributed to the increasing in the amount of polymeric vanadyl species. When V loading exceeds 10, crystalline bulk V_2O_5 starts to cover the surface of the samples, which causes their intrinsic catalytic activities to be decreased. Thus, the higher activity of V_m/MO_x catalysts in the soot combustion reaction with respect to polymeric vanadyl species arise from the formation of easily reducible ''surface oxide species'' ensuring an easier occurrence of the redox cycle under reaction conditions [32]. Therefore, the medium-loading (V_4/MO_x or V_{10}/MO_x) catalysts have the highly catalytic performances for soot combustion. By contrast, high loading V_m/MO_x systems exhibit a poor catalytic performance in soot combustion in spite of their high density of reduced sites. V_4/TiO_2 is the most active catalyst in essence among all of V_m/MO_x samples. Furthermore, A_4V_4/TiO_2 catalysts are more active than V_4/TiO_2 catalyst in essence due to their stronger redox reactivities characterized by H_2-TPR.

4.2. The controlling factors for soot catalytic combustion

Oxygen supply by a surface oxide with redox properties seems to be necessary to obtain an active catalyst for soot combustion [13]. On the basis of TPR and FT-IR results described above, some considerations on the reaction mechanism of soot combustion over A_4V_4/MO_x-type catalysts can be made. It is well known that the activity of the vanadium oxide in combustion reaction is closely related to the reactivity of the oxygen in the V–O–M bond. The oxygen exchange rate of catalysts based on transition metal oxides, in particular VO_x, is found to be improved by doping alkali metals, which is ascribed to their electron-donating effect of the alkali metals that enhanced the reactivity of V–O bonds. Moreover, it is also observed that alkali can weaken the C–C bonds and promote the formation of C–O bonds during catalytic combustion [33–35]. Therefore, the catalytic activity after adding alkali metals should be attributed to the synergetic effect of these ones and V–O bonds, which are simultaneously present in the vanadyl structures. The role of the electron-donating effect of alkali metals agrees with our experimental results. TPR results show that the decrease of the reduction temperature of the vanadium species in the presence of alkali metal, which suggests a weakening of the V–O or V=O bond. Furthermore, FT-IR measurement results reveal that the addition of alkali to VO_x shift the V=O stretching vibration to lower wave number, which also reflects that the V=O bond stretching vibration becomes weaker. The catalytic activity has been successfully correlated with the redox ability of the A_4V_4/MO_x catalysts for the combustion reaction of soot. A_4V_4/TiO_2 samples show higher catalytic activities for soot combustion compared with other V_m/MO_x samples. Moreover, the IR results show that AVO_3 and A_2CO_3 are present in the A_4V_4/TiO_2 systems. In a word, the spectroscopic analysis and H_2-TPR results suggest that the higher activity of alkali-promoted vanadium oxide catalysts can be related to the ability of alkali metal promoting the redox cycle of the active vanadium oxide species.

It should be mentioned that the TPR profiles indicate that the reducibility of V_m/TiO_2 is much lower than those of V_m/Al_2O_3 or V_m/SiO_2. Nevertheless, its activity is higher than others. This indicates that even though the redox capacity is essential to the soot combustion activity, there is no direct correlation between the bulk reducibility as obtained from TPR and the activity comparing with different supports. This is because, in addition to the total reducibility of the active phase, its contact with the soot particle is another important factor for the total reaction. V_m/ZrO_2 and V_m/TiO_2 catalysts have much higher tight contact activities than the V_m/Al_2O_3 and V_m/SiO_2 catalysts. It is due to the lower melting points and the larger density of surface active sites of V_m/ZrO_2 and V_m/TiO_2 than those of V_m/Al_2O_3 and V_m/SiO_2 catalysts. Furthermore, for the A_4V_4/TiO_2 system, the catalytic activity for soot combustion is not always consistent with their redox abilities determined by TPR. However, there is a good correlation between the melting point of these samples and the catalytic activity according to the TG results. Low melting points can ensure the good surface atom migration ability, which would improve the contact between the catalyst and soot. Thus, the mobility of catalysts is another important factor for soot combustion.

In general, an ideal soot combustion catalyst should be considered from the following aspects. First of all, it should be a strong redox material, i.e., it has a high intrinsic catalytic activity. Secondly, its surface atoms should retain a good mobility

attributing to its low melting point or other factors. This synergy between strong redox property and good mobility of catalyst is a fundamental role for promoting soot combustion.

5. Conclusions

(1) An ideal soot combustion catalyst should be consisted of a compound with a strong redox property and a good mobility of surface atoms. On the one hand, the polyvanadate species are the more active redox sites for soot combustion than the isolated monovanadate species and crystalline V_2O_5. On the other hand, low melting points can ensure the good surface atom migration ability, which would improve the contact between catalyst and soot.
(2) Doping alkali metals into supported vanadium oxide catalysts can enhance their redox properties. In addition, alkali metals improve the contact between catalyst and soot due to their low melting points. Thus, alkali-promoted vanadium oxide catalysts can remarkably improve the catalytic activity for soot combustion. The catalytic activity order for soot combustion followed Li > Na > K > Rb > Cs comparing with the different alkali metal doped catalysts.
(3) Support nature also has large influences on the structure and catalytic activity of supported vanadium oxide catalysts. The activity order follows: Ti > Zr > Al > Si over these V_m/MO_x catalysts. And Li_4V_4/TiO_2 catalyst gave the best activity for soot combustion in the A_4V_4/TiO_2 system, i.e., the lowest reaction temperature. T_{10}, T_{50}, and T_{90} were 299, 347, and 377 °C, respectively.

Acknowledgements

This work was supported by the National Natural Science Foundation of China (No. 20473053), the Beijing Natural Science Foundation (No. 2062020), the Scientific Research Key Foundation for the Returned Overseas Chinese Scholars of State Education Ministry, and the National Basic Research Program of China (Grant No. 2004CB217806).

References

[1] G. Mul, F. Kapteijn, J.A. Moulijn, Appl. Catal. B 12 (1997) 33.
[2] Z. Zhao, A. Obuchi, J. Oi-Uchisawa, A. Ogata, S. Kushiyama, Chem. Lett. 4 (1998) 367.
[3] L.E. Briand, O.P. Tkachenko, M. Guraya, X. Gao, I.E. Wachs, W. Grunent, J. Phys. Chem. B 108 (2004) 4823.
[4] Z. Zhao, Y. Yamada, A. Ueda, H. Sakurai, T. Kobayashi, Catal. Today 93–95 (2004) 163.
[5] Z. Zhao, X. Gao, I.E. Wachs, J. Phys. Chem. B 107 (2003) 6333.
[6] X. Gao, J.L.G. Fierro, I.E. Wachs, Langmuir 15 (1999) 3169.
[7] A. Khodakov, J. Yang, S. Su, E. Iglesia, A.T. Bell, J. Catal. 177 (1998) 343.
[8] J. Liu, Z. Zhao, C. Xun, A. Duan, L. Zhu, X. Wang, Appl. Catal. B 61 (2005) 39.
[9] G. Neri, G. Rizzo, S. Galvagno, M.G. Musolino, A. Donato, R. Pietropaolo, Thermochim. Acta 381 (2002) 165.
[10] B.A.A.L. Van Setten, J.M. Schouten, M. Makkee, J.A. Moulijn, Appl. Catal. B 28 (2000) 253.
[11] P.A.J. Neeft, M. Makkee, J.A. Moulijn, J. Chem. Eng. 64 (1996) 295.
[12] R. Jimenez, X. Garcia, C. Cellier, P. Ruiz, A.L. Gordon, Appl. Catal. A 297 (2006) 125.
[13] E.E. Miro, F. Ravelli, M.A. Ulla, L.M. Cornaglia, C.A. Querini, Catal. Today 53 (1999) 631.
[14] V. Serra, G. Saracco, C. Badini, V. Specchia, Appl. Catal. B 11 (1997) 329.
[15] C.A. Querini, L.M. Cornagia, M.A. Ulla, E.E. Miro, Appl. Catal. B 20 (1999) 165.
[16] F. Roozeboom, M.C. Mlttelmeljer-Hazeleger, J.A. Mouljn, J. Medema, V.H.J. De Beer, P.J. Gellings, J. Phys. Chem. B 84 (1980) 2783.
[17] B.M. Weckhuysen, I.E. Wachs, in: H.S. Nalwa (Ed.), Handbook of Surface and Internalface of Materials, Surface and Internalface Pressure, vol. 1, Academic Press, 2002 (Chapter 11).
[18] B.M. Reddy, B. Chowdhury, I. Ganesh, E.P. Reddy, T.C. Rojas, A. Fernandez, J. Phys. Chem. B 102 (1998) 10176.
[19] F. Prinetto, G. Ghiotti, M. Occhiuzzi, V. Indovina, J. Phys. Chem. B 102 (1998) 10316.
[20] Z. Zhao, Y. Yamada, Y. Teng, A. Ueda, K. Nakagawa, T. Kobayashi, J. Catal. 190 (2000) 215.
[21] C. Cristiani, P. Forzatti, G. Busca, J. Catal. 116 (1989) 595.
[22] W.P. Griffith, T.D. Wickins, J. Chem. Soc. A (1969) 1066.
[23] J. Laane, J.R. Ohlsen, Prog. Inorg. Chem. 27 (1980) 465.
[24] V.G. Milt, C.A. Querini, E.E. Miro, M.A. Ulla, J. Catal. 220 (2003) 424.
[25] L. Zhu, X. Wang, J. Yu, Z. Hao, Acta Phys. Chim. Sin. 21 (2005) 840.
[26] X. Gao, M.A. Banares, I.E. Wachs, J. Catal. 188 (1999) 325.
[27] M.A. Larrubia, G. Busca, Mater. Chem. Phys. 72 (2001) 337.
[28] X. Gao, I.E. Wachs, J. Phys. Chem. B 104 (2000) 1261.
[29] F. Prinetto, G. Ghiotti, M. Occhiuzzi, V. Indovina, J. Phys. Chem. B 102 (1998) 10316.
[30] B. Olthof, A. Khodakov, A.T. Bell, E. Iglesia, J. Phys. Chem. B 104 (2000) 1516.
[31] B.M. Reddy, B. Chowdhury, I. Ganesh, E.P. Reddy, T.C. Rojas, A. Fernandez, J. Phys. Chem. B 102 (1998) 10176.
[32] V. Sokolovskii, F. Arena, S. Coluccia, A. Parmaliana, J. Catal. 173 (1998) 238.
[33] J. Liu, Z. Zhao, C.M. Xu, Acta Phys. Chim. Sin. 21 (2005) 156.
[34] G. Saracco, C. Badini, N. Russo, V. Specchia, Appl. Catal. B 21 (1999) 233.
[35] A.L. Carrascull, M.L. Ponzi, E.N. Ponzi, Ind. Eng. Chem. Res. 42 (2003) 692.